Soliton states from quadratic electron-phonon interaction

Zhongjin Zhang , ¹ Anatoly Kuklov, ² Nikolay Prokof'ev , ¹ and Boris Svistunov , ¹ Department of Physics, University of Massachusetts, Amherst, Massachusetts 01003, USA
² Department of Physics and Astronomy, CSI, and the Graduate Center of CUNY, New York, New York 10314, USA
³ Wilczek Quantum Center, School of Physics and Astronomy and T. D. Lee Institute, Shanghai Jiao Tong University, Shanghai 200240, China

(Received 20 September 2023; accepted 21 November 2023; published 11 December 2023)

We present a numerically exact study of self-trapped (also referred to as soliton) states of electrons that form in materials with strong quadratic coupling to the phonon coordinates. Previous studies failed to observe predictions based on the variational approach in continuum space because soliton states form only when system parameters are taken to the extreme limit. At the variational level, we establish that finite-radius solitons emerge through the weak first-order transition as the coupling strength is increased, and subsequently collapse to the single-site state through a strong first-order transition. Both transitions transform into smooth crossovers between the light and heavy polaron states in the full quantum treatment. The most surprising effect not observed in other polaron models is the nonmonotonic dependence of the soliton effective mass and the residue at strong coupling.

DOI: 10.1103/PhysRevB.108.245127

I. INTRODUCTION

For decades, studies of polarons—electrons renormalized by their coupling to lattice vibrations [1–3]—were focused on the linear density-displacement electron-phonon interaction (EPI),

$$H_{\rm int} = \sum_{\mathbf{k}\mathbf{q}\sigma\alpha} V_{\mathbf{q}\alpha} c_{\mathbf{k}-\mathbf{q}\sigma}^{\dagger} c_{\mathbf{k}\sigma} [b_{\mathbf{q}\alpha}^{\dagger} + b_{-\mathbf{q}\alpha}], \tag{1}$$

where α is the phonon branch index (we use standard notations for the creation and annihilation operators for electrons $c_{\mathbf{k},\sigma}^{\dagger}$, $c_{\mathbf{k}\sigma}$ and phonons $b_{\mathbf{q}\alpha}^{\dagger}$, $b_{-\mathbf{q}\alpha}$ in momentum representation). The most popular models were the local Holstein [4,5] and the nonlocal Frohlich [6,7] models with $V_{\mathbf{q}\alpha}=$ const and $V_{\mathbf{q}\alpha}\propto 1/q$, respectively (for a recent review, see Ref. [8]). More recently, researchers started exploring alternative interaction mechanisms based on the electron hopping amplitude dependence on atomic displacements [9–15] that bring an additional dependence of the vertex function in (1) on the incoming electron momentum, $V_{\mathbf{q}\alpha} \to V_{\mathbf{k},\mathbf{q}\alpha}$, but remain linear in the phonon coordinates. The interest in new models was motivated by their unusual properties and the possibility of having light but compact bipolarons (bound states of two electrons) with a high superconducting transition temperature [13,16].

The properties of polarons with quadratic EPI remained much less explored and understood:

$$H_{\text{int}} = g_2 \frac{\Omega}{4} \sum_{\mathbf{i}} n_{\mathbf{i}} [b_{\mathbf{i}}^{\dagger} + b_{\mathbf{i}}]^2. \tag{2}$$

Here, Ω is the local oscillator frequency in the absence of coupling; it changes to $\tilde{\Omega} = \sqrt{1 + g_2 n_i} \Omega$ when the site is occupied. Note the crucial dependence of the model's properties on the sign of g_2 and, in particular, the instability taking place at $g_2 < -1$.

An intriguing regime emerges when the two limits, $\Omega \to 0$ and $g_2 \to +\infty$, conspire to preserve finite $\tilde{\Omega}$. Indications of the importance of this regime were found in several materials: doped manganites [17], halide perovskites [18], and quantum paraelectrics [19,20]. The soft vibration modes in these materials are transverse optical phonons for which the linear EPI is suppressed in the long-wave limit [21–25]; similar physics takes place in optically pumped systems [26,27]. Early suggestions that biphonon exchange could be an important pairing mechanism at low doping [21] were recently revisited and used to explain superconductivity in SrTiO₃ [28–30]. However, dealing with nonlinear couplings theoretically beyond perturbation theory has been challenging. The original work [22–25] was based on the variational solution for large-radius soliton states in continuum. The momentum average approximation [31] was used to study a combination of linear and nonlinear EPI in Refs. [32,33]. More recently, nonlinear EPI effects were investigated in Refs. [34–36] using the determinant Monte Carlo method [37] for finite twodimensional (2D) systems at high electron density and finite temperature. Finally, the interplay between the linear and quadratic EPI in continuum was studied in Ref. [38] by the variational Feynman's path-integral method [39].

The situation has changed with the development of the numerically exact x-representation Monte Carlo (XMC) technique for polaron problems with arbitrary nonlinear density-displacement and arbitrary sign-preserving hopping-displacement interactions [40]. It was used to obtain the precise results for quadratic EPI (2) at strong coupling [41], but the study failed to observe soliton states predicted by one of the authors in Refs. [22,23] despite considering a relatively small adiabatic parameter $\gamma = \Omega/W = 1/48$, where W = 12t is the bandwidth of the 3D tight-binding model on the cubic lattice with the nearest-neighbor hopping amplitude t. Thus, no progress on the soliton problem was made for more than three decades, and it remains unknown how and under

what conditions these states form and what are their basic properties.

In this paper, we first expand the variational analysis of the adiabatic limit to reveal how solitons form and then collapse in first-order phase transitions. Next, we present results of the numerically exact studies of solitons by the XMC method in the parameter regime that is orders of magnitude beyond the limitations of other known schemes: $\gamma = 1/600$ and $\gamma = 1/2400$ with g_2 as large as 10^8 . In the full quantum solution, the first-order transitions are transformed into smooth crossovers with an unusual (not observed in other polaron problems) nonmonotonic dependence of the effective mass and Z factor on g_2 at strong coupling.

II. HAMILTONIAN, EFFECTIVE ADIABATIC MODEL, AND METHODS

The full system's Hamiltonian on the simple cubic lattice reads

$$H = 6t - t \sum_{\langle ij \rangle} c_i^{\dagger} c_j + \Omega \sum_i b_i^{\dagger} b_i + H_{\text{int}}.$$
 (3)

(The phonon energy is counted from the ground state of the unperturbed harmonic oscillator.) In the adiabatic, $\gamma \to 0$, limit one takes advantage of the fact that electrons are much faster than phonons and the contribution of the latter to energy depends solely on the average electron density distribution [1,2,22,23]. For model (3), these standard considerations lead to the following energy functional to be minimized:

$$E = 6t - t \sum_{\langle ij \rangle} \psi_i^* \psi_j + \frac{\Omega}{2} \sum_i (\sqrt{1 + g_2 |\psi_i|^2} - 1).$$
 (4)

Here, ψ is the normalized electron wave function (real for the ground state), and the last term is the sum of ground-state energies for each oscillator. Given that oscillator frequencies increase with g_2 , the adiabatic condition for the polaron of radius R is satisfied if $\sqrt{R^{-3}g_2}\Omega \ll t/R^2$ or $g_2 \ll (t/\Omega)^2/R$ (the lattice constant a=1 serves as the unit of length). For a large-radius soliton, we also consider a continuous counterpart of Eq. (4) with m=1/2t:

$$E = \int d^3r \left[\frac{1}{2m} |\nabla \psi|^2 + \frac{\Omega}{2} (\sqrt{1 + g_2 |\psi|^2} - 1) \right].$$
 (5)

Minimization of Eq. (4) is achieved by the gradient descent method when at each stage the wave function is first transformed according to $\tilde{\psi} = \psi - \epsilon \nabla_{\psi} H$ and then normalized to unity. This step is rejected and the value of ϵ is decreased by a factor of two if $E[\tilde{\psi}] > E[\psi]$; otherwise it is accepted. For optimal solutions we record their energies and root-mean-square radii, $R = \sqrt{\langle r^2 \rangle}$, where $\langle r^2 \rangle = \sum_i r_i^2 \psi_i^2$. We ensure that all finite-size effects are exponentially small for the polaron solutions presented in this paper (realistically, one can work with about 300³ sites after utilizing system symmetries).

Numerically exact solutions of (3) are obtained using the recently developed XMC method based on the lattice path integral for the electron and coordinate representation for harmonic oscillators (see Refs. [40,41] for a complete description). Key polaron properties, such as the dispersion relation, E_p , ground-state energy, $E = E_{p=0}$, effective mass,

 $1/m^* = d^2 E_{p=0}/dp^2$, and the quasiparticle residue, $Z = Z_{p=0}$, are obtained from simulations of the polaron Green's function, $G_p(\tau)$, and its asymptotic behavior, $G_p(\tau) \rightarrow Z_p e^{-E_p \tau}$, in the $\tau \rightarrow \infty$ limit.

III. VARIATIONAL ANALYSIS

The formation of solitons is driven by competition between the hopping term favoring delocalized states and EPI repulsion preferring localized states due to the sublinear dependence of the interaction energy on density at strong coupling [last terms in (4) and (5)]. Since delocalized states correspond to $\psi_i \rightarrow 0$, their variational energy readily follows from Eq. (4) in this limit: $E_0 = g_2 \Omega/4$.

Localized continuous solutions at strong coupling were obtained in Refs. [22,23]. If the last term in (5) is approximated as $\Omega\sqrt{g_2}|\psi|/2$, then energy minimization reduces to the solution of the radial eigenvalue equation, $-d^2\psi/dr^2 + m\Omega\sqrt{g_2}/2 - \lambda\psi = 0$, with the solution

$$\psi(r) = \sqrt{\frac{3}{10\pi R_A^3}} \left[1 - \frac{R_A \sin(x_0 r / R_A)}{r \sin(x_0)} \right],\tag{6}$$

for $r < R_A$ and $\psi(r) = 0$ for $r \ge R_A$, where $x_0 \approx 4.49$ is the lowest positive root of $\tan x = x$ and R_A is the cutoff radius, $R_A = [6x_0^4/(5\pi g_2\Omega^2 m^2)]^{1/7}$. The root-mean-square radius of this solution is given by $R = (11/25 - 49/10x_0^2)^{1/2}R_A \approx 0.444R_A$ and its energy

$$E_A = \frac{7}{10} \left(\frac{5\pi x_0^3}{6} \right)^{2/7} \frac{(g_2 \Omega^2)^{2/7}}{m^{3/7}} \approx 3.34 \frac{(g_2 \Omega^2)^{2/7}}{m^{3/7}}$$
 (7)

falls below $g_2\Omega/4$ for $g_2 > 37.7(m\Omega)^{-3/5}$.

Thus, on the one hand, solitons form at strong coupling $g_2\gg 1$. On the other hand, this coupling needs to be small enough to ensure adiabaticity of the state and its large radius because at $g_2>(t/\Omega)^2$ both conditions are violated. At $g_2\gg (t/\Omega)^2$ the polaron state is well described by the so-called atomic limit (AL) when the electron changes frequency only of the harmonic oscillator at the occupied site (see Ref. [41]). Physically, this is a completely different state characterized by $R\approx 0$ and $E_{\rm atom}\approx \frac{\Omega}{2}(\sqrt{1+g_2}-1)$.

In a more precise treatment, the last term in (5) is dealt with "as is" and the cutoff at R_A gets replaced with the gradual exponential decay of the wave function with distance; this feature is important for a correct description of the transition between the localized and delocalized states. The corresponding numerical analysis is presented below. In the absence of a hard cutoff, we have to resort to the root-mean-square radii for defining the polaron size.

To study the properties of solitons away from the asymptotic adiabatic limit ($\gamma \to 0$, $R \to \infty$)—how they first form and then transition to the AL state—we resort to the exact minimization of the lattice functional (4) by gradient descent, the results are shown in Figs. 1 and 2. Using t=1 as the energy unit, we first consider the case of an extremely small phonon frequency $\Omega/t=10^{-5}$ (see Fig. 1). For $g_2\gg g_c$ ($g_c=26\,406$), both E and R are accurately described by the asymptotic continuous solutions. However, this is no longer the case on approach to g_c , because exact variational solutions remain stable at significantly smaller (by a factor of two)

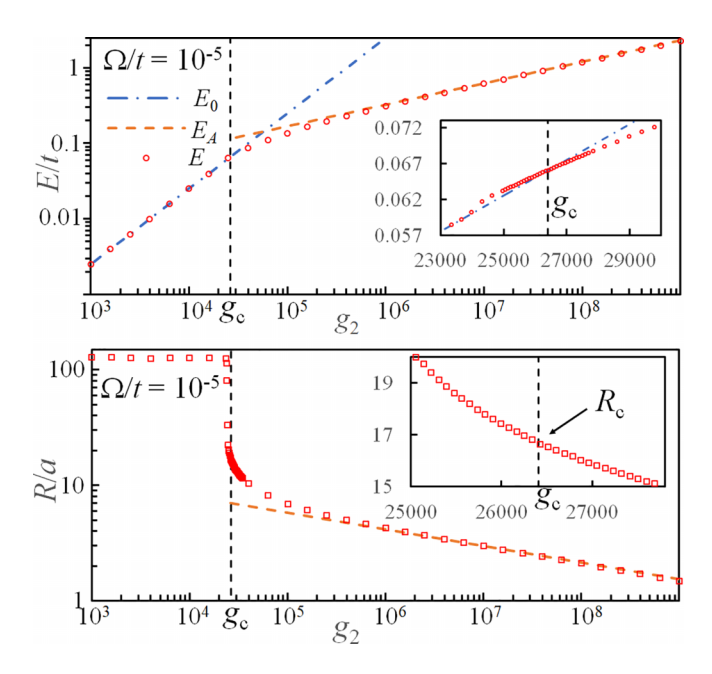


FIG. 1. Energy (upper panel, red circles) and radius (lower panel, red squares) of lattice variational states as functions of g_2 for $\Omega/t = 10^{-5}$. Dashed (orange) lines are the asymptotic continuous solutions [see Eq. (7) and the text above]. The dashed-dotted (blue) line is the energy of the delocalized state. Insets: Energy and radius vs g_2 near the critical point.

values of g_2 as their volume undergoes a rapid expansion (by nearly an order of magnitude). This is a clear indication that the hard-cutoff approximation is not reliable near the critical point.

A close examination of the $|g_2 - g_c|/g_c \ll 1$ region (see the insets in Fig. 1) reveals that within the variational treatment, solitons with a finite radius R_c emerge through a weak first-order transition. Indeed, for g_2 slightly smaller than g_c , we detect metastable localized solutions (obtained by starting from an initial wave function with a small radius), which subsequently disappear at $g_2 < 0.92g_c$. The phase transition point can be located very accurately from the intersection of the E and E_0 curves.

In continuum, the energy functional is invariant under the scaling transformation, $r \to br$, $g_2 \to b^3 g_2$, $\Omega \to b^{-3} \Omega$, and $m \to b^{-2}m$. Moreover, if m and Ω are changed while keeping the adiabatic parameter $m\Omega$ constant, the functional is simply multiplied by a factor $\tilde{\Omega}/\Omega$. Thus, upon proper scaling, we are left with only one free parameter, g_2 . These considerations imply that the critical coupling and radius scale as $g_c \propto (m\Omega)^{-3/5}$ and $R_c \propto (m\Omega)^{-1/5}$. On a lattice, this scaling is expected to fail when $R_c \sim a$. Data in Fig. 3 demonstrate the accuracy of this prediction for large critical sizes.

IV. QUANTUM SOLUTION

For a less extreme but still small adiabatic ratio $\gamma = 1/600$ we are posed to compare variational and full quantum solutions (see Fig. 2). As expected, the first-order transition at $g_c = 272.7$ predicted by (4) is replaced with a smooth quantum crossover. Despite the very small value of γ the exact energy is still significantly different from its

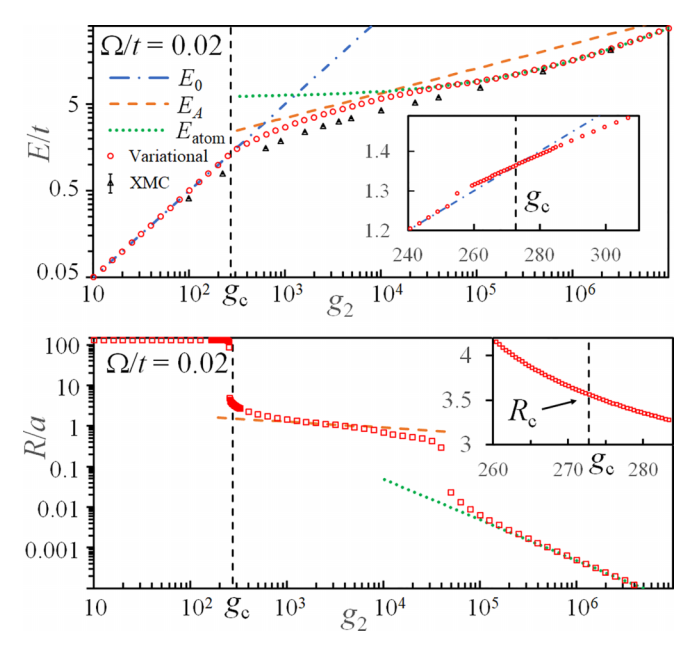


FIG. 2. Upper panel: Energies of variational states (red circles) in comparison with XMC results (black triangles) for $\Omega=0.02$. Lower panel: Variational state radii (red squares). Dashed (orange) lines are predictions of the asymptotic continuous solutions. The dashed-dotted (blue) line is the energy of the delocalized variational state E_0 . The dotted (green) line is the atomic limit energy $E_{\rm atom}$. Inset: Variational E vs g_2 near the critical point.

variational counterpart across the crossover region. This surprising outcome finds its explanation in the relatively small soliton sizes predicted by (4): about four lattice spacings at g_c and quickly shrinking to $R \sim a$ in a broad parameter range. Quantum effects are expected to be pronounced at the lattice scale, not to mention that for $R \sim a$ the adiabatic condition also becomes questionable. Nevertheless, it is clear that at $g_2 \sim 10^3$ the polaron state undergoes a radical transformation from a perturbative plane-wave state with a slightly renormalized effective mass and $Z \approx 1$ to a state with m^*/m much larger and a Z factor much smaller than what is expected in the AL (see Fig. 4). These results imply that the electron is

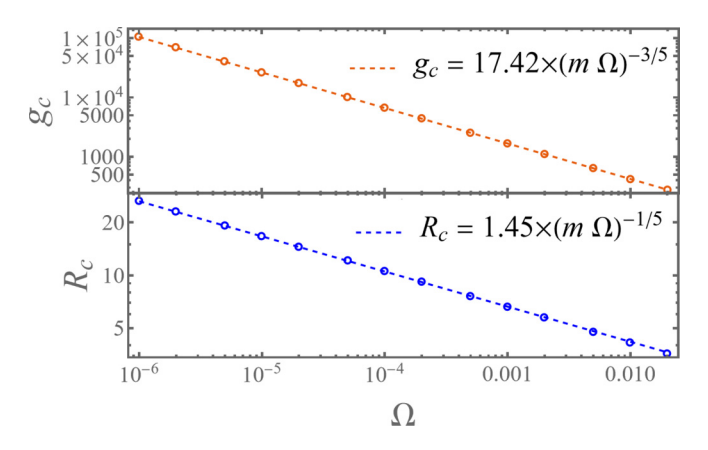


FIG. 3. Critical coupling and radius of solitons in continuum as a function of Ω . Both show a clear power-law dependence (dashed lines) with expected exponents.

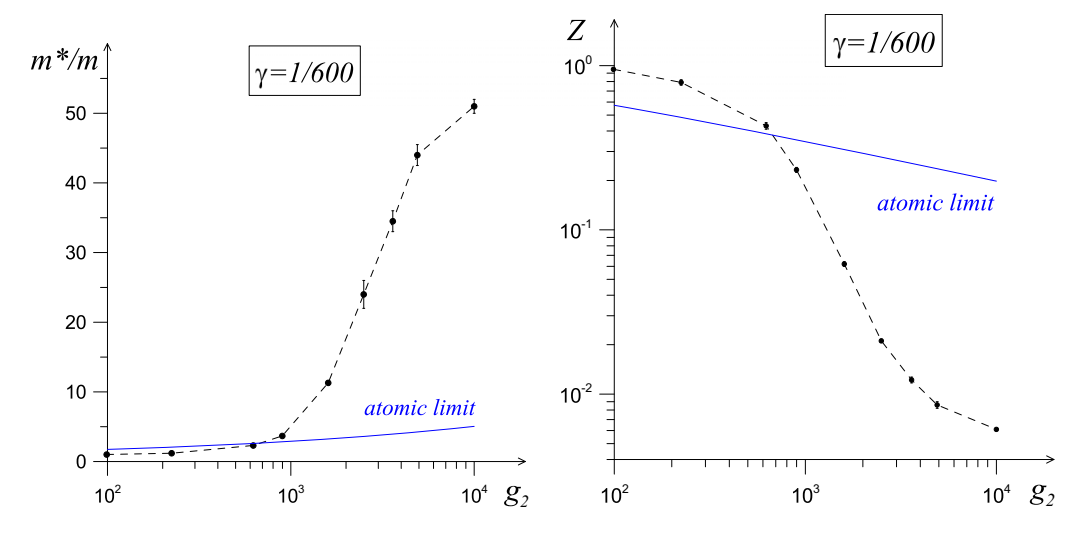


FIG. 4. Effective mass and Z factor for $\Omega/t = 0.02$ as functions of g_2 from the XMC method. Solid lines are results expected in the atomic limit.

"dressed" by oscillator excitations distributed over multiple sites, i.e., it forms a soliton.

We observe that the parameters required for the formation of large-radius solitons are extreme and well beyond the limits of applicability of other unbiased methods. For XMC, simulations of $\gamma < 0.001$ are also very challenging in the regime of large effective masses, $m^*/m \gtrsim 1000$, and exponentially small Z factors. This explains why previous numerical studies failed to see them.

V. COLLAPSE TO THE ATOMIC LIMIT: LIGHTER POLARONS AT STRONGER COUPLING

Once solitons form, their radius gradually decreases with coupling and at $g_2 \sim (t/\Omega)^2$ both lattice effects and nonadiabatic corrections come into play. Naive expectations are that AL is nothing but the end of the smooth monotonic evolution of the soliton state. This turns out to be incorrect and in a rather dramatic fashion. Figure 2 shows that the lattice functional features a second transition at large g_2 , this time between the soliton and AL states. It can be understood analytically by restricting analysis to just two wave-function components near the transition point: $\psi_0 \simeq 1$ at the center and $\psi_1 \ll 1$ at the six nearest-neighbor sites (other components are proportional to higher powers of ψ_1). By assuming that $\psi_1^2 g_2 \gg 1$ and using the normalization condition, $\psi_0^2 = 1 - 6\psi_1^2$, we arrive at the energy dependence on ψ_1 ,

$$E/t = 6[6\psi_1^3 - \chi\psi_1^2 + 2(\chi - 1)\psi_1] + \text{const},$$
 (8)

that features a first-order transition when $\chi = \sqrt{g_2}\Omega/(4t) = \chi_c$, with $\chi_c \approx 1.022$. At this level of description, the transition is from small but nonzero ψ_1 at $\chi < \chi_c$ to $\psi_1 = 0$ at $\chi > \chi_c$. In terms of the coupling constant, the transition takes place at $g_2 > (4t/\Omega)^2 = 9/\gamma^2$. [The above consideration is valid only in the $\gamma \to 0$ limit; more precise treatment with terms $\propto \chi/(g_2\psi_1)$ included shows that the discontinuous transition to the AL takes place only for $\gamma < 0.0015$].

While there is no reason to trust variational results for compact states, they do point to the possibility of having a much faster crossover to the AL than what is expected in terms of a slow power-law evolution $R \propto g_2^{-1/7}$. Given an order of magnitude difference between the effective masses and Z factors of the soliton and AL states (see Fig. 4), a monotonic power-law transformation of one state into another would require enormous values of g_2 . But if this transformation takes the form of a more rapid crossover, then m^* and Z must exhibit a nonmonotonic dependence on g_2 at strong coupling. Such highly counterintuitive behavior was not reported for other polaron problems. By extending XMC simulations to much larger values of g_2 for $\gamma = 1/600$ and performing additional simulations for $\gamma = 1/2400$ at strong coupling, we do observe the nonmonotonic dependence of m^* and Z (more pronounced for smaller γ) (see Fig. 5), i.e., solitons are getting lighter as they approach AL.

VI. CONCLUSIONS

We performed detailed studies of soliton states in the model with a strong quadratic electron-phonon interaction by (i) extending a previous variational analysis to lattice systems, (ii) revealing two first-order transitions and their properties, which explain how solitons form and subsequently collapse to the single-site states at the variational level, and (iii) solving the problem numerically exactly by the *x*-representation Monte Carlo technique. In exact solutions, transitions are replaced by smooth crossovers with a rapid increase of the effective mass and decrease of the quasiparticle residue at strong coupling. An opposite trend is discovered when the soliton size is of the order of the lattice spacing.

Previous numerical work failed to see solitons because they form when system parameters take values way beyond the limitations of other unbiased methods. Future work should explore the properties of bipolaron states in the same model; bound states are expected to form in the same parameter regime where solitons form and for the same reason—a

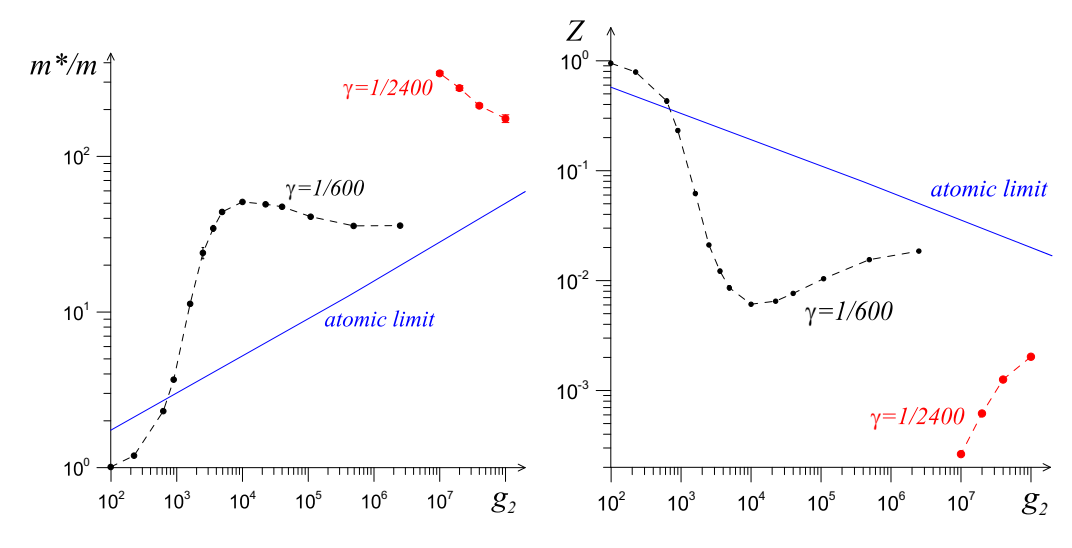


FIG. 5. Effective masses and Z factors for $\Omega/t = 0.02$ and $\Omega/t = 0.005$ as functions of g_2 over a much broader range that in Fig. 4. Solid lines are results expected in the atomic limit.

sublinear dependence of the interaction energy on electron density. Figure 5 suggests that it is possible to have light and compact bipolarons, which is a prerequisite for a high superconducting temperature at finite density [13,16].

ACKNOWLEDGMENT

We acknowledge support from the National Science Foundation under Grants No. DMR-2032136 and No. DMR-2032077.

- [1] L. Landau, Phys. Z. Sowjetunion 3, 664 (1933).
- [2] S. Pekar, Zh. Eksp. Teor. Fiz. 16, 335 (1946).
- [3] L. Landau and S. Pekar, Zh. Eksp. Teor. Fiz. 18, 419 (1948).
- [4] T. Holstein, Ann. Phys. 8, 325 (1959).
- [5] T. Holstein, Ann. Phys. 281, 725 (2000).
- [6] H. Fröhlich, H. Pelzer, and S. Zienau, Philos. Mag. 41, 221 (1950).
- [7] H. Fröhlich, Adv. Phys. 3, 325 (1954).
- [8] C. Franchini, M. Reticcioli, M. Setvin, and U. Diebold, Nat. Rev. Mater. 6, 560 (2021).
- [9] D. J. J. Marchand, G. De Filippis, V. Cataudella, M. Berciu, N. Nagaosa, N. V. Prokof'ev, A. S. Mishchenko, and P. C. E. Stamp, Phys. Rev. Lett. 105, 266605 (2010).
- [10] J. Sous, M. Chakraborty, R. V. Krems, and M. Berciu, Phys. Rev. Lett. 121, 247001 (2018).
- [11] B. Xing, W.-T. Chiu, D. Poletti, R. T. Scalettar, and G. Batrouni, Phys. Rev. Lett. 126, 017601 (2021).
- [12] C. Zhang, N. V. Prokof'ev, and B. V. Svistunov, Phys. Rev. B 104, 035143 (2021).
- [13] C. Zhang, J. Sous, D. R. Reichman, M. Berciu, A. J. Millis, N. V. Prokof'ev, and B. V. Svistunov, Phys. Rev. X 13, 011010 (2023).
- [14] M. R. Carbone, A. J. Millis, D. R. Reichman, and J. Sous, Phys. Rev. B 104, L140307 (2021).
- [15] J. Sous, C. Zhang, M. Berciu, D. Reichman, B. Svistunov, N. Prokof'ev, and A. Millis, arXiv:2210.14236.
- [16] C. Zhang, B. Capogrosso-Sansone, M. Boninsegni, N. V. Prokof'ev, and B. V. Svistunov, Phys. Rev. Lett. 130, 236001 (2023).
- [17] V. Esposito, M. Fechner, R. Mankowsky, H. Lemke, M. Chollet, J. M. Glownia, M. Nakamura, M. Kawasaki, Y. Tokura,

- U. Staub, P. Beaud, and M. Först, Phys. Rev. Lett. **118**, 247601 (2017).
- [18] M. Schilcher, P. Robinson, D. Abramovitch, L. Tan, A. Rappe, D. Reichman, and D. Egger, ACS Energy Lett. 6, 2162 (2021).
- [19] A. Kumar, V. I. Yudson, and D. L. Maslov, Phys. Rev. Lett. 126, 076601 (2021).
- [20] K. G. Nazaryan and M. V. Feigel'man, Phys. Rev. B 104, 115201 (2021).
- [21] K. L. Ngai, Phys. Rev. Lett. 32, 215 (1974).
- [22] A. Kuklov, Phys. Lett. A 139, 270 (1989).
- [23] A. B. Kuklov, Superconductivity **3**, S355 (1990) [Sverkh-provodimost (KIAE) **3**, 2277 (1990)].
- [24] A. Gogolin and A. Ioselevich, Pis'ma Zh. Eksp. Teor. Fiz. 53, 456 (1991) [JETP Lett. 53, 479 (1991)].
- [25] A. Gogolin and A. Ioselevich, Pis'ma Zh. Eksp. Teor. Fiz. 54, 291 (1991) [JETP Lett. 54, 285 (1991)].
- [26] D. Kennes, E. Wilner, D. Reichman, and A. Millis, Nat. Phys. 13, 479 (2017).
- [27] J. Sous, B. Kloss, D. Kennes, D. Reichman, and A. Millis, Nat. Commun. 12, 5803 (2021).
- [28] D. van der Marel, F. Barantani, and C. W. Rischau, Phys. Rev. Res. 1, 013003 (2019).
- [29] P. Volkov, P. Chandra, and P. Coleman, Nat. Commun. 13, 4599 (2022).
- [30] D. E. Kiselov and M. V. Feigel'man, Phys. Rev. B 104, L220506 (2021).
- [31] M. Berciu, Phys. Rev. Lett. 97, 036402 (2006).
- [32] C. Adolphs and M. Berciu, Europhys. Lett. **102**, 47003 (2013).
- [33] C. P. J. Adolphs and M. Berciu, Phys. Rev. B 89, 035122 (2014).
- [34] S. Li and S. Johnston, Europhys. Lett. **109**, 27007 (2015).

- [35] S. Li, E. A. Nowadnick, and S. Johnston, Phys. Rev. B **92**, 064301 (2015).
- [36] P. Dee, J. Coulter, K. Kleiner, and S. Johnston, Commun. Phys. **3**, 145 (2020).
- [37] S. Johnston, E. A. Nowadnick, Y. F. Kung, B. Moritz, R. T. Scalettar, and T. P. Devereaux, Phys. Rev. B 87, 235133 (2013).
- [38] M. Houtput and J. Tempere, Phys. Rev. B 103, 184306 (2021).
- [39] R. P. Feynman, Phys. Rev. 97, 660 (1955).
- [40] N. V. Prokof'ev and B. V. Svistunov, Phys. Rev. B **106**, L041117 (2022).
- [41] S. Ragni, T. Hahn, Z. Zhang, N. Prokof'ev, A. Kuklov, S. Klimin, M. Houtput, B. Svistunov, J. Tempere, N. Nagaosa, C. Franchini, and A. S. Mishchenko, Phys. Rev. B 107, L121109 (2023).